PROCEEDINGS OF SCIENCE

ZEPLIN-III

Timothy J Sumner[*†]
Imperial College London
E-mail: t.sumner@imperial.ac.uk

ZEPLIN-III is a 12 kg two-phase xenon time projection chamber used to search for the weakly interacting massive particles (WIMPs) that may account for the dark matter of our Galaxy. The detector measures both scintillation and ionisation produced interactions in the liquid to differentiate between nuclear recoils expected from WIMPs and electron recoil background signals down to ∼10 keV nuclear recoil energy. This paper reviews the science results obtained from the first science run and reports on the current status of the upgrade and second science run. The first science run obtained 847 kg·days of data acquired between February 27^{th} 2008 and May 20^{th} 2008 and excluded a WIMP-nucleon elastic scattering spin-independent cross-section above 8.1×10^{-8} pb at 60 GeVc^{-2} with a 90% confidence limit. ZEPLIN-III demonstrated better discrimination at low-energy than previously achieved by any other xenon-based experiments and highlighted a non-linearity in the low-energy response to nuclear recoils. The upgrade includes replacement of the PMT array and the addition of an active veto for gammas and neutrons. The second science run should offer an order of magnitude improvement in sensitivity.

Identification of Dark Matter 2010-IDM2010
July 26-30, 2010
Montpellier France

[*]Speaker.

[†]On behalf of the ZEPLIN-III collaboration: Edinburgh University, Imperial College London, ITEP Moscow, LIP-Coimbra and STFC-RAL.

1. Introduction

Searches for weakly interacting massive particles (WIMPs) are motivated by the coming together of unification schemes, such as supersymmetry, predicting new particles, and extensive observational evidence for additional non-baryonic gravitational mass in the Universe. That WIMPs of supersymmetry naturally fulfill this need is remarkably persuasive, and they also occur in other frameworks. They interact non-gravitationally with baryonic matter via a weak interaction. Low event rates and energy deposits: $<$0.1 events/day/kg and $<$50 keV dictate the use of underground experiments capable of identifying energy deposits due to elastic scattering of WIMPs from target nuclei.

ZEPLIN-III is the latest in a series of instruments [1, 2, 3]. The design and performance details of the two-phase (liquid/gas) xenon time-projection chamber can be found elsewhere [4, 5]. The active volume is a $\sim$12 kg disc of liquid xenon (35 mm$\times$190 mm) above an array of 31 2-inch diameter photomultipliers [6] which record a fast scintillation signal, S1, and a delayed signal, S2, from gas phase proportional electroluminescence [7]. Electric fields, defined by a cathode wire grid 36 mm below the liquid surface and an anode plate 4 mm above the surface, provide the drift field in the liquid (3.9 kV/cm), the surface extraction field, and the gas electroluminescence field (7.8 kV/cm). The fiducial volume is defined by the S1 to S2 time delay and by 2-D position reconstruction to select a radial boundary at 150 mm. Time delays from 500-13,000 ns select depths between 1.29-33.43 mm, to give a 6.5 kg fiducial volume. Signals were sampled at 2 ns by two 8-bit digitisers (ACQIRIS DC265) with a $\times$10 gain difference for high and low sensitivity readout. The PMT array operates from a common HV with variable attenuators to normalise gains. A trigger uses the shaped sum signal from all PMTs. S2 causes the trigger at $\sim$11 ionisation electrons corresponding to S1$\sim$0.2 keVee referenced to the equivalent S1 signal produced by 122 keV γ-rays.

The xenon vessel and outer vacuum jacket were made from low-background OFHC copper. Cooling is provided by a 40 litre LN2 reservoir inside the vacuum jacket. Thermal stability to $<$0.5 ^{o}C is achieved by controlled flow of nitrogen boil-off gas through a cooling flange. Pressure stability to 2% was maintained. A shield with 30 cm polypropylene and 20 cm lead gave 10^5 attenuation for external γ-rays and neutrons.

2. The First Science Run

847 kg·days of data were collected over 83 days continuous operation from 27^{th} Feb 2008. ^{57}Co calibrations were done every day. Nuclear recoil calibrations were made with an AmBe neutron source.

Pulses in waveforms were classified as S1 or S2 candidates based on pulse width: S1 pulses are shorter ($\tau\lesssim$40 ns) than S2 pulses with widths equal to the gas drift time ($\tau\sim$550 ns). Software thresholds were applied ($\geq$3 PMTs above 1/3 photoelectron for S1 and a minimum area of $\sim$5 ionisation electrons for S2). Only events with one S1-S2 pair were accepted. χ^2 fit indicators from position reconstruction were used to remove multiple-scatter events. Double-Compton scatters with a vertex in a 'dead' region are referred to as 'multiple-scintillation single-ionisation' (MSSI) events.

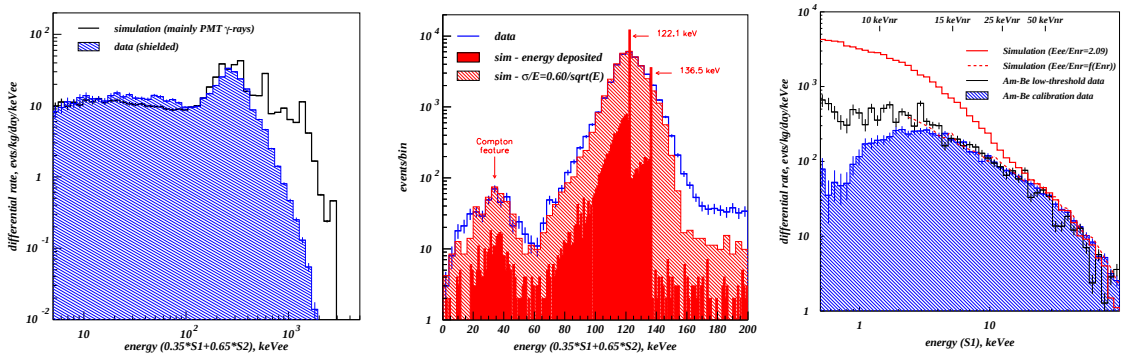

Figure 1: Left: Measured electron recoil background differential spectrum, together with a Monte Carlo prediction [4] using GEANT4 [14]. The latter includes 10.5 evts/kg/day/keVee ('dru') from the photomultipliers. The disagreement at high energies is caused by single-scatter selection in the data (but not in the simulation) and by the limited DAQ dynamic range. Middle: One day's ^{57}Co calibration in the combined anti-correlation energy channel (blue). A simulation is in red:the solid histogram shows actual energy deposits and the shaded one has been convolved with the energy resolution. Right: Differential energy spectra for the AmBe nuclear recoil populations. The main calibration data (shaded blue histogram) and the lower threshold data-set (black) are compared with the Monte Carlo simulation using a constant conversion factor between keVee and keVnr (solid red curve). The ratio between these two curves is interpreted as an efficiency factor. The dashed red curve allows for the nuclear recoil non-linearity analysis.

2.1 Calibration

An external ^{57}Co source was placed above the instrument every day. A typical ^{57}Co spectrum is shown in Figure 1(middle). The S1 light detection efficiency was 1.8 p.e./keVee, decreasing from 5.0 p.e./keVee at zero electric field. The 122 keV signals were used for many purposes. With S2, an iterative procedure flat-fielded the response of the PMT array. Radial position reconstruction used converged response profiles in simultaneous least-squares minimisation to all channels [8]. This complemented Monte Carlo template matching [9]. S1 and S2 areas gave light collection correction factors as a function of radial position. Using these, a full-volume energy resolution of σ=5.4% at 122 keV was obtained (Figure 1(Middle)). ^{57}Co data were well fitted to simulations including a Compton feature at $\sim$35 keV. The daily calibrations were used to monitor operational parameters over the run: i) the average light and ionisation yields; ii) the mean electron lifetime; iii) detector tilt. The mean light and ionisation yields remained stable to a few percent. The lifetime improved from an initial value of 20 μs to 35 μs at the end. The nuclear recoil response was calibrated with an AmBe (α,n) source. Figure 2 shows a 'scatter-plot' of $\log_{10}(S2/S1)$. A fit to the median of the distribution with $\pm 1\sigma$ boundaries is shown. Data were histogramed in 1 keVee bins and fitted by log-normal distributions. The population between 40–70 keVee is inelastic scattering from ^{129}Xe. The electron-recoil response was established from a ^{137}Cs calibration. Populations in the ^{137}Cs and WIMP-search data-sets were both well fitted in 1 keVee bins by a skew-Gaussian function. Fit parameters are consistent bin-by-bin, but with two differences in general behaviour. First, the mean of the Cs data is systematically lower, caused by PMT gain suppression at the high count rate needed [10]. Second, the behaviour of MSSI in the Cs data-set is not closely representative of the science data. Hence, instead of using the ^{137}Cs data, the WIMP-search data themselves were used

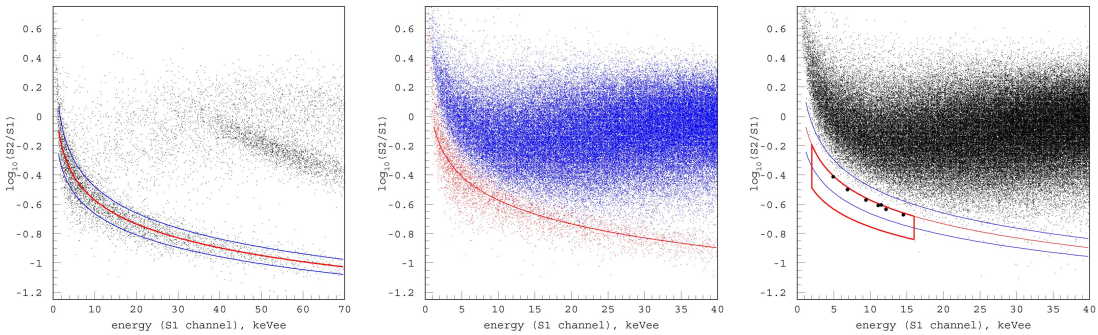

Figure 2: Left: Calibration of the nuclear recoil response with an AmBe neutron source, plotted as the discrimination parameter ($\log_{10}(S2/S1)$) as a function of S1 keVee. The lines show the mean and standard deviation of log-normal fits to the population. The distinct population above ∼40 keVee is inelastic neutron scattering off ^{129}Xe. Middle: Combined scatter plot from the two calibration data-sets, ^{137}Cs and AmBe. Right: Scatter plot of $\log_{10}(S2/S1)$ as a function of S1 keVee for the 83-day data-set. There are 7 events (large dots) in the WIMP-search region (thick red box).

to estimate the expected electron-recoil background, and this gave 11.6±3.0.

The nuclear recoil population is used to define the WIMP search box with boundaries $2<E<16$ keVee and $(\mu_n - 2\sigma)<\log_{10}(S2/S1)<\mu_n$, (acceptance of 47.7%).
Background predictions are based on a full GEANT4 [14] simulation including measured radioactive content levels for all major components [4]. The largest contributor is the PMT array. Figure 1(right) shows the measured differential background spectrum together with the simulated background. The expected single-scatter neutron background in the data-set is 1.2 ± 0.6 in the WIMP search box with 90% coming from PMT (α,n) interactions and spontaneous fission.

2.2 Analysis of the WIMP Search Data

Figure 2(right) shows the final scatter plot which demonstrates a discrimination level of 5×10^3 between 2–16 keVee increasing below 5 keVee. XENON10 achieved 99.9% at the very lowest energies [11] whilst our data show >99.99% in the 2-5 keVee band.

Detection efficiency is a combination of hardware trigger and software effects, including pulse finding algorithms and selection cuts, which are expected to appear ∼S1=2 keVee. This was confirmed by a second AmBe data-set acquired with a 50% S2 trigger threshold and analysed with the 3-fold S1 coincidence requirement reduced to 2-fold and all software quality cuts significantly relaxed. This is shown in Figure 1(right) by comparing the 'Am-Be low-threshold data' with the 'Am-Be calibration data'. The difference between these two is only noticeable below S1∼4 keVee as expected. The smallest S2 triggers in each run were ∼11 and ∼4 ionisation electrons, respectively, calibrated against the single electron spectrum [18]. The experiment efficiency is the ratio of the two AmBe data-sets. The full curve labelled 'Simulation (Eee/Enr=2.09)' in Figure 1(right) is a Monte Carlo simulation of the expected differential spectrum assuming a constant ratio between keVee and keVnr. It is clear that a departure from the experimental data extends well above 4 keVee. This has been used to derive the conversion between keVee and keVnr. The conversion allows for energy dependence in the combination of the 'quenching' factor and the field suppression of the scintillation output. Above E_{nr}∼20 keV data for the quenching factor suggests it is

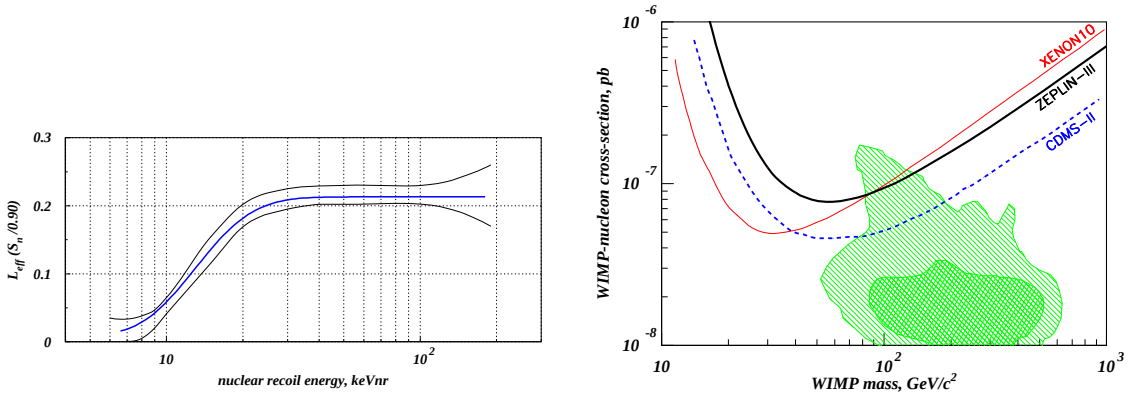

Figure 3: Left: the derived energy-dependent behaviour. The middle curve shows the best fit, with the band enclosing other curves producing acceptable fits, but should not be interpreted as a 1σ band. Right: 90% two-sided upper limit to the WIMP-nucleon elastic scattering cross-section for a spin-independent interaction. Results from XENON10 [11, 24] and CDMS-II [25] are shown. The XENON10 curve is a 1-sided limit, corresponding to an 85% confidence 2-sided limit [11]. Hatched areas show 68% and 95% confidence regions with flat priors calculated in CMSSM [26].

constant at $\sim$0.19 [15, 16, 17]. At lower energies the situation is much less clear [13]. There are no data on energy dependence of the field suppression but rather a single datum from a measurement at 56 keVnr using a neutron beam [16]. Using a maximum-likelihood technique we derived a non-linearity function which best matches the AmBe simulation to our neutron calibration spectrum above $\sim$2 keVee. Figure 3(right) shows the nonlinearity function. The band shown is indicative of the uncertainty in the function but is not formally a 1σ uncertainty band which would likely be somewhat wider. The non-linearity found is more significant than that reported by the XENON10 experiment [13] and subsequent independent beam measurements have confirmed this tendancy [19]. The WIMP search box boundaries are at 10.7 and 30.2 keVnr. The events in the box are close to where an electron background is expected. Although there is a good fit of a skew-Gaussian to this background above the box, there is a systematic uncertainty in its extrapolation into the box. The best fit expectation exceeds the measured number of events, which might result in an artificially low upper limit [20]. Hence, a simpler, more conservative approach is used based on three pieces of information. The first is that an electron-recoil background would preferentially fall in the top part of the WIMP search box. Hence the box is divided into two regions having significantly different background expectations. The search box is transformed into nuclear recoil acceptance percentiles so that any WIMP signal should populate the box uniformly. The second is that there are no WIMP events in the lower region. Finally, there are up to 7 WIMP events in the upper region. A classical 90% one-sided upper limit for the whole box WIMP expectation value, μ, is that for which 10% of repeated experiments would return no events in the lower box and up to 7 in the upper box. For the fractional area, f, in the range 0.75 to 0.84, Poisson probabilities give $\mu = 2.30/f$, driven by the empty region. The two-sided 90% confidence interval is also driven by the empty region and is $\mu = 2.44/f$ [20]. With $f = 0.8$ the 90% upper limit is $\mu = 3.05$ and $\mu = 0$ is included within the two-sided interval. An upper limit to the WIMP-nucleon spin-independent elastic scattering cross-section, following [21] and using the Helm form factor [22]. The upper

limit, shown in Figure 3, has a minimum of 8.1×10^{-8} pb at a WIMP mass of 60 GeV/c^2. Spin-dependent limits are presented in [27].
Significant new constraints on inelastic dark matter, iDM, have been derived using the higher energy data from the nuclear recoil band and these rule out that scenario as an explanation for the annual modulation seen by the DAMA experiment at at least very an 88% confidence levels [28] over the whole parameter space.

3. The Upgrade and Second Science Run

A number of planned upgrades have now been made to the experiment and a second science run has started. The upgrades should allow ZEPLIN-III to improve its sensitivity by an order of magnitude [4]. The upgrades include:-

- Replacement of the PMT array with customised pin-compatible PMTs made from lower background materials. ET Enterprises Ltd.[1], supplied the original PMTs from their standard product range and then worked on a lower background variety which could straightforwardly replace them. These were made from fully screened materials and used novel quartz/metal seals to significantly reduce their radioactivity budget. The result of this can be seen in Figure 4.

- A plastic veto system has been installed which replaces, and substitutes for, part of the passive polypropylene shielding. The veto has both gamma-ray and neutron tagging capability at the 30% and 65% levels respectively [29]. The lowest curve in Figure 4 shows the spectrum of background events which are identified by a prompt tag in the veto as gamma-rays. The efficiency with which the veto is tagging gamma-rays is $\sim$ 30%. Delayed neutron tagging has an efficiency of $\sim$ 65%

- A shadow grid has been installed above the top anode mirror. Absorption by the grid produces a marked suppression in counts from the ^{57}Co calibration source allowing the position reconstruction algorithms to be improved. Figure 4 shows a image with both actual data (left-hand side) and simulated data (right-hand side). The resolution obtained in the position reconstruction is better than 2mm fwhm.

- An automated source positioning system has been installed to ensure calibrations are reproducible and that any rate-dependent PMT response sagging can be properly corrected for.

- A new calibrated AmBe source is being used for neutron calibration to allow the low-energy response to be further studied.

- An LED pulser signal with fibre-optic feed into detector volume has been incorporated to enable in situ PMT gain monitoring.

The second science run started on June 23rd 2010 and science data are being collected with a 96% efficiency. At the start of the run the electron lifetime was 20μs and, as seen in the first science

[1] http://www.et-enterprises.com

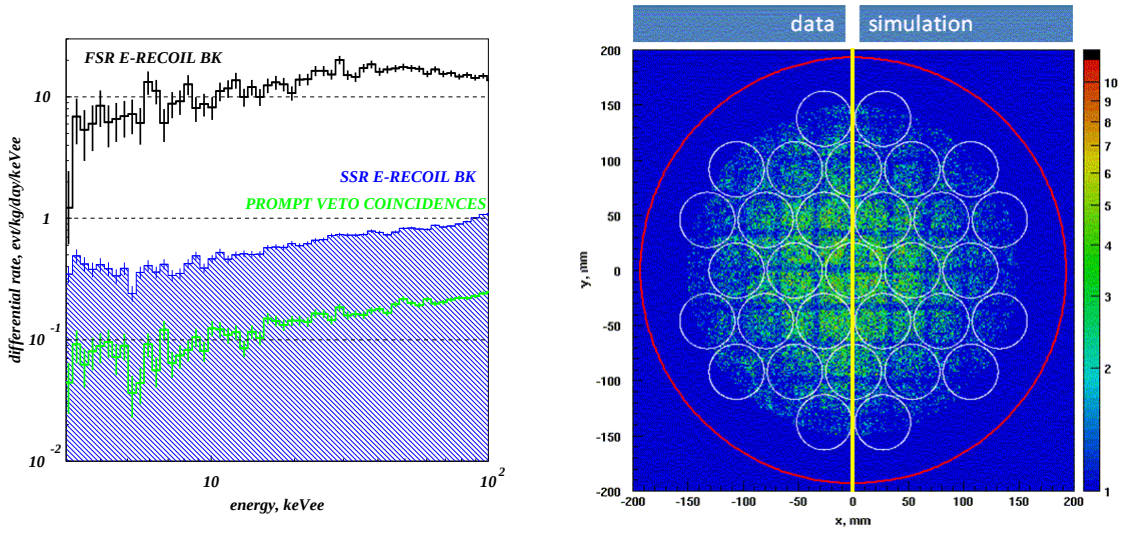

Figure 4: Left: the gamma-ray backgrounds seen during the first science run (black - top curve) compared with that seen during the second science run (blue - middle curve). The lowest curve shows the background spectrum of events having a prompt gamma tag from the veto system. Right: A ^{57}Co calibration run showing the effect of the shadow grid. The left-hand side of this composite image shows the actual data, whilst the right-hand side shows a simulation.

run, it has steadily improved to around 30μs at present. The target exposure for this second run is $\sim$3000 kg.days which should allow a sensitivity improvement of about an order of magnitude [4].

References

[1] G.J. Alner *et al.*, Astropart. Phys. **23**, 444 (2005)

[2] G.J. Alner *et al.*, Astropart. Phys. **28**, 287 (2007)

[3] V.N. Lebedenko *et al.*, Phys. Rev D, **80**, 052010 (2009)

[4] H.M. Araújo *et al.*, Astropart. Phys. **26**, 140 (2006)

[5] D.Yu. Akimov *et al.*, Astropart. Phys. **27**, 46 (2007)

[6] H.M. Araújo *et al.*, Nucl. Instrum. Meths. A **521**, 407 (2004)

[7] B.A. Dolgoshein, V.N. Lebedenko, B.U. Rodionov, JETP Lett.**11** 513 (1970)

[8] V.N. Solovov *et al.*, In preparation (2010)

[9] A. Lindote *et al.*, Nucl. Instrum. Meths. A **573**, 200 (2007)

[10] F. Neves *et al.*, Astropart. Phys. **33**, 13 (2010)

[11] J. Angle *et al.*, Phys. Rev. Lett. **100**, 021303 (2008)

[12] T. Shutt *et al.*, Nucl. Phys. B Proc. Suppl. **173**, 160 (2007)

[13] P. Sorensen *et al.*, Nucl. Instrum. Meths. A **601**, 339 (2009)

[14] S. Agostinelli *et al.*, Nucl. Instrum. Meths. A **506**, 250 (2003)

[15] D. Akimov *et al.*, Phys. Letts. B **524**, 245 (2002)

[16] E. Aprile *el al.*, Phys. Rev. D **72**, 072006 (2005)

[17] V. Chepel *el al.*, Astropart. Phys. **26**, 58 (2006)

[18] B. Edwards *et al.*, Astropart. Phys. **30**, 54 (2008)

[19] A. Manzur *et al.*, Phys. Rev. C **81**, 025808 (2010)

[20] G.J. Feldman, R.D. Cousins, Phys. Rev. D **57**, 3873 (1998)

[21] J.D. Lewin, P.F. Smith, Astropart. Phys. **6**, 87 (1996)

[22] R.H. Helm, Phys. Rev. **104**, 1466 (1956)

[23] L. Roszkowski, R. Ruiz de Austri, and R. Trotta, J. High Energy Phys. **07**, 075 (2007)

[24] E. Aprile *el al.*, Phys. Rev. C **79**, 045807 (2009)

[25] Z. Ahmed *et al.*, Phys. Rev. Letts. **102**, 011301 (2009)

[26] R. Trotta *et al.*, J. High Energy Phys. **12**, 24 (2008)

[27] V.N. Lebedenko *et al.*, Phys. Rev. Letts. **103**, 151302 (2009)

[28] D.Yu Akimov *et al.*, Phys. Letts. B **692**, 180 (2010)

[29] D.Yu Akimov *et al.*, Astropart. Phys. **34**, 151 (2010)